Weakly nonlinear analysis of short-wave elliptical instability

Savio B. Rodrigues[1] and Jayme De Luca[2]
[1]*Department of Mathematics, Federal University at São Carlos, UFSCar, Caixa Postal 676, São Carlos, São Paulo 13565-905, Brazil*
[2]*Department of Physics, Federal University at São Carlos, UFSCar, Caixa Postal 676, São Carlos, São Paulo 13565-905, Brazil*

(Received 15 October 2008; accepted 9 December 2008; published online 27 January 2009)

Two-dimensional inviscid flows with elliptical streamlines have linearly unstable three-dimensional modes close to the center of the ellipse. The linear instability equilibrates in the presence of enough viscosity, yielding a continuous set of neutrally stable plane waves known as Craik–Criminale waves (CCWs). For initial disturbance in a discrete superposition of plane waves our weakly nonlinear analysis yields a cubic ordinary differential equation for the slow-time evolution of the neutrally stable plane-wave amplitudes. In the subcritical region we find that all solutions eventually vanish, while in the supercritical region the amplitudes either saturate or have exponential growth; the existence of a finite-time blowup at cubic order being unlikely. The saturation to a steady state is possible only for special initial conditions, and for generic initial conditions the amplitudes saturate to a chaotic state. In contrast, a single CCW with exponential growth is still unstable, but it loses stability to cycles of growth and decay among the plane waves. © *2009 American Institute of Physics*. [DOI: 10.1063/1.3068188]

I. INTRODUCTION

Elliptical streamlines are generally associated with a vortex subject to a straining field (shear) in either laminar or turbulent flows. The linear instability of flows with elliptical streamlines is called elliptical instability.[1] In the short-wave limit, elliptical instability has a local character, i.e., only the local shape of the streamlines is important for the instability. The model for the theory is a basic flow where the velocity field is a superposition of a rigid-body rotation and a linear straining field. The basic flow may have circular, elliptic, straight, or hyperbolic streamlines, depending on the strength of rotation and strain. Here we consider only elliptic streamlines where the linear instability gives rise to the three-dimensional (3D) universal modes studied by Pierrehumbert.[2] This linear instability was later described by Bayly[3] in terms of a parametric instability of the plane-wave solutions, $\mathbf{v}(t)e^{i\mathbf{k}(t)\cdot\mathbf{x}}$, known as Craik–Criminale waves (CCWs).[4] Furthermore, Landman and Saffman[5] showed that the parametric instability is stabilized if there is enough viscosity. In another study, Lifschitz and Hameiri[6] used geometrical optics to derive evolution equations for localized high-frequency disturbances, $\mathbf{v}(\mathbf{x},t)e^{i\phi(\mathbf{x},t)/\epsilon}$, of a basic flow with general velocity fields (possibly time dependent). The asymptotic solution leads to a transport equation for the phase $\phi(\mathbf{x},t)$ and an ordinary differential equation (ODE) for the velocity amplitude $\mathbf{v}(t,\mathbf{x}(t;\mathbf{x}_0))$ along streamlines (the same amplitude equation that is found for a CCW). In particular, when the streamline is the stagnation point in the center of a steady two-dimensional vortex, geometrical optics implies the linear instability *and* the nonlinear instability[6,7] of elliptical flows. The geometrical-optics asymptotics has been justified rigorously[8] and, in a suitable norm, a small 3D high-frequency disturbance with fast decaying envelope becomes as large as the basic flow.

Here we apply a weakly nonlinear analysis to a discrete superposition of neutrally stable CCWs in a viscous flow with elliptical streamlines. The neutrally stable plane-wave solutions are perturbed away from the neutral curve[5] and the wave amplitudes change in a slow-time scale. We derive the cubic nonlinear ODE for the wave amplitudes using an asymptotic procedure with two time scales. In the subcritical region we find that wave amplitudes eventually vanish. In the supercritical region, the wave amplitudes either saturate to bounded amplitudes or grow at most exponentially fast. A finite-time blowup of the wave amplitudes was never observed in our numerical calculations. In a few special cases we have proven that a finite-time blowup does not exist for the cubic equations. Our results suggest that it is unlikely that cubic nonlinear effects could lead to a fast transition to turbulence. The saturation to a steady state is possible only when the dynamics is initialized in a suitable subspace, e.g., a superposition of CCWs with the same wave amplitude. In contrast, for generic superpositions of CCWs the wave amplitudes saturate to a chaotic state with no dominant feature.

Since a CCW is an exact solution of the Navier–Stokes equation (NSE), the cubic-order equations have an exponential solution for initial condition in a single CCW. For our model flow, the single CCW solution grows unbounded in the supercritical region. When the single CCW is perturbed by other CCWs with small amplitudes, we find that the original CCW loses stability to cycles of growth and decay of each wave amplitude in the superposition. The numerical studies show that the resulting disturbance does not grow as fast as a single CCW. To our knowledge, the growth-and-decay cycles found here have not been observed either in experiments or in direct numerical simulations (DNS). We conjecture that the growth-and-decay cycles could be reproduced in a DNS with a multiphase disturbance with a slowly

 © 2009 American Institute of Physics

Downloaded 17 Nov 2009 to 200.136.239.153. Redistribution subject to AIP license or copyright; see http://pof.aip.org/pof/copyright.jsp

varying envelope. Our model does not include mean-flow interactions and therefore is valid only if the initial-disturbance envelope is flat enough for the mean-flow corrections to be of a higher asymptotic order. Another limitation of our weakly nonlinear analysis is the failure to treat the extreme cases where the elliptical streamlines are either circular or degenerate into parallel lines (rigid body rotation and shear flow, respectively).

In a rotating elliptical tank, the connection between weakly nonlinear saturation and secondary instability has been studied in detail.[9] In contrast to elliptical flows, a finite-time blowup can be found in the weakly nonlinear dynamics of global modes in a rotating circular tank with periodic compression along its axis.[10] The secondary instability of a CCW in an inviscid flow has been studied using geometrical optics,[11] where the instabilities have wavelengths much shorter than the wavelength of the CCW. The transition to chaos involving the interactions of CCWs has been addressed using the fully nonlinear equations;[12] as the viscosity is decreased, the route to chaos through period doubling is described in detail for a superposition involving three resonant CCWs. Here we extend the equations of Ref. 12 to a superposition involving more modes with a weakly nonlinear dynamics close to the critical Reynolds number. Last, short-wave stability shows agreement with classical linear stability studies with flattened Taylor–Green vortices[13,14] and, in recent comparisons, it shows favorable results.[15,16]

This paper is divided as follows. In Sec. II we give the basic equations and review known results. In Sec. III we derive the ODE for the slow-time evolution of the amplitudes of the neutrally stable waves, first for a four-wave resonance and then for a superposition with many waves. In Sec. IV we discuss the stability of the wave amplitudes, i.e., the stability of a CCW, the type of bifurcation, and the existence of a finite-time blowup. In Sec. V we have the discussions and conclusion. Appendix A brings a technical proof and Appendix B details the numerical analysis of our main equation, a very stiff ODE.

II. BASIC EQUATIONS AND RESULTS

The basic flow considered here has elliptical streamlines in 3D space without boundaries. The basic flow is $\mathbf{U}^*(\mathbf{x}^*)=A^*\mathbf{x}^*$ with

$$A^*=\begin{bmatrix} 0 & -\gamma^*-\mu^* & 0 \\ \gamma^*-\mu^* & 0 & 0 \\ 0 & 0 & 0 \end{bmatrix}, \tag{1}$$

where a star is used to denote dimensional quantities. The parameter $\gamma^*\geq 0$ sets the rotation rate and μ^* sets the strain rate, $0\leq\mu^*<\gamma^*$. Rigid-body rotation is attained with $\mu^*=0$, while $\mu^*=\gamma^*$ is a shear flow. The vorticity of the basic flow is $\mathbf{W}^*=[0,0,2\gamma^*]^t$. We introduce an adimensionalization where the total flow is given by $\mathbf{U}(\mathbf{x})+\mathbf{u}(\mathbf{x},t)$, and where $\mathbf{U}(\mathbf{x})\equiv A\mathbf{x}$ with $A=A^*/\gamma^*$; the total vorticity is $\mathbf{W}(\mathbf{x})+\omega(\mathbf{x},t)$ with $\mathbf{W}=[0,0,2]^t$. The vorticity formulation of the NSE is

$$\partial_t\omega+\mathbf{U}\cdot\nabla\omega+\mathbf{u}\cdot\nabla\omega-\mathbf{W}\cdot\nabla\mathbf{u}-\omega\cdot\nabla\mathbf{U}-\omega\cdot\nabla\mathbf{u}=\nu\Delta\omega, \tag{2}$$

together with $\omega=\nabla\times\mathbf{u}$ and $\nabla\cdot\mathbf{u}=0$. The adimensional parameters are the strain to rotation ratio $\beta=\mu^*/\gamma^*$, $0<\beta<1$, and Reynold's number, $\mathrm{Re}=\nu^{-1}$, with $\nu=\nu^*k_0^2/\gamma^*$, where k_0 is chosen as the wavenumber of the initial condition and ν^* is the dimensional viscosity. Since the basic flow is a model for a region of a global flow, there is a length scale L where the global flow can be regarded as slowly varying in space. The initial wavelength should be much smaller than L, i.e., $k_0L\gg 2\pi$.

The CCW is an exact solution of Eq. (2) with the form

$$\omega(\mathbf{x},t)=\mathbf{w}(t)e^{i\mathbf{k}(t)\cdot\mathbf{x}}+\text{c.c.}, \tag{3}$$

$$\mathbf{u}(\mathbf{x},t)=\mathbf{v}(t)e^{i\mathbf{k}(t)\cdot\mathbf{x}}+\text{c.c.}, \tag{4}$$

where c.c. denotes the complex conjugate of the preceding expression. The equation for $\mathbf{k}(t)$ is

$$\dot{\mathbf{k}}=-A^t\mathbf{k}, \tag{5}$$

and the equation for $\mathbf{w}(t)$ is

$$\dot{\mathbf{w}}+\mathcal{L}(\mathbf{k})\mathbf{w}+\nu\|\mathbf{k}\|^2\mathbf{w}=0, \tag{6}$$

where

$$\mathcal{L}(\mathbf{k})\mathbf{w}=(\mathbf{W}\cdot\mathbf{k})\frac{\mathbf{k}\times\mathbf{w}}{\|\mathbf{k}\|^2}-A\mathbf{w}, \tag{7}$$

with $\mathbf{w}(0)\cdot\mathbf{k}(0)=0$. Since the vector fields are divergence-free ($\nabla\cdot\omega=0$ and $\nabla\cdot\mathbf{u}=0$), the vector amplitudes $\mathbf{w}(t)$ and $\mathbf{v}(t)$ are related by the expressions $\mathbf{w}(t)=i\mathbf{k}(t)\times\mathbf{v}(t)$ and

$$\mathbf{v}(t)=\frac{i\mathbf{k}(t)\times\mathbf{w}(t)}{\|\mathbf{k}(t)\|^2}, \tag{8}$$

so that $\mathbf{k}(t)\cdot\mathbf{w}(t)=0$ and $\mathbf{k}(t)\cdot\mathbf{v}(t)=0$. The solution of Eq. (5) is

$$\mathbf{k}(t)=[k_x(t),k_y(t),k_z(t)]^t=k_0[\sin\theta\cos\Omega(t-s),\alpha\sin\theta\sin\Omega(t-s),\cos\theta]^t, \tag{9}$$

where $\Omega=\sqrt{1-\beta^2}$, $\alpha=\sqrt{(1+\beta)/(1-\beta)}$, and s and θ are arbitrary real numbers (with ν defined as above we can assume $k_0=1$). Furthermore, $\mathbf{k}(t)$ has period $P=2\pi/\Omega$ and the solution is such that k_z is always constant while $[k_x(t),k_y(t)]$ describe an ellipse (with the same eccentricity as the streamlines but with the longer axis in the y-direction). Since Eq. (6) has periodic coefficients, we only need to solve it for the $s=0$ case of Eq. (9). Using the Floquet theory, the solution of Eq. (6) is a linear combination of three Floquet modes $e^{\sigma_jt}\mathbf{p}_j(t)$, $j=1,2,3$; where each $\mathbf{p}_j(t)$ has period P and the Floquet exponents are ordered with $\mathrm{Re}(\sigma_1)\geq\mathrm{Re}(\sigma_2)\geq\mathrm{Re}(\sigma_3)$. Let

$$\rho(\beta,\nu)=\max_{0\leq\theta\leq\pi/2}\mathrm{Re}(\sigma_1(\theta,\beta,\nu)) \tag{10}$$

and let $\theta(\beta,\nu)$ be the angle that yields this maximum. Figure 1 shows the regions of stability $\rho(\beta,\nu)<0$, instability

Downloaded 17 Nov 2009 to 200.136.239.153. Redistribution subject to AIP license or copyright; see http://pof.aip.org/pof/copyright.jsp

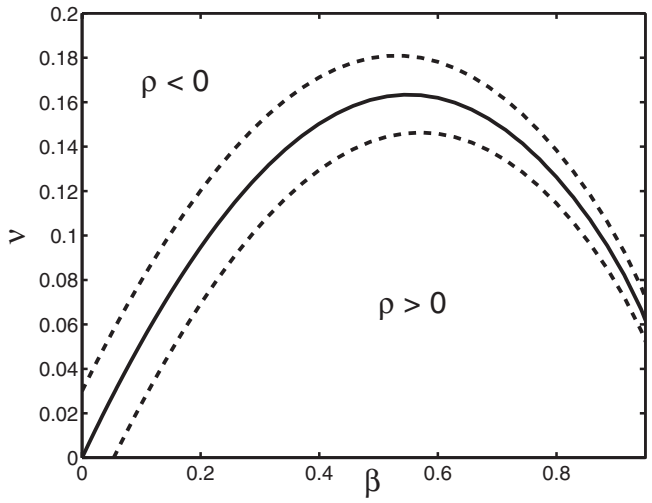


FIG. 1. Regions of stability, $\rho<0$, and instability, $\rho>0$, are divided by the neutral curve $\rho(\beta,\nu_c)=0$ (solid line). The dashed lines indicate the level curves $\rho=\pm 0.03$.

$\rho(\beta,\nu)>0$, and the neutral curve $\rho(\beta,\nu)=0$ as described by Landman and Saffman[5] (where the vertical axis was chosen to be $2\pi\nu$). Each β defines a *critical viscosity* ν_c such that $\rho(\beta,\nu_c)=0$, and a *critical angle* $\theta_c=\theta(\beta,\nu_c)$. Each β also defines a continuous set of *critical wavevectors* $\mathbf{k}^c(t)$, henceforth denoted with a superscript c, given by Eq. (9) with $k_0=1$, $\theta=\theta_c$, and $s\in[0,P)$. If $\mathrm{Re}(\sigma_1)=0$, it can be shown[5] that $\mathrm{Im}(\sigma_1)=0$ and $\mathrm{Re}(\sigma_j)<0$ for $j=2,3$. Thus, on the neutral curve, there is a continuous set of neutrally stable Floquet modes parametrized by s, $\mathbf{w}(t)=\mathbf{p}_1(t-s)$. The function $\mathbf{p}_1(t)$ is sinusoidal with a subharmonic relation among its components: $\mathbf{p}_{1x}(t-P/2)=\mathbf{p}_{1x}(t)$, $\mathbf{p}_{1y}(t-P/2)=\mathbf{p}_{1y}(t)$, and $\mathbf{p}_{1z}(t-P/2)=-\mathbf{p}_{1z}(t)$.

III. WEAKLY NONLINEAR ASYMPTOTICS

We seek an asymptotic solution of Eq. (2) with an initial condition given by a superposition of plane waves. We consider β and ν close to the point (β,ν_c) on the neutral curve (Fig. 1) and expand ν about ν_c as $\nu=\nu_c+\epsilon^2\nu_2$, where ϵ is the perturbation parameter. The Ansatz for the weakly nonlinear asymptotic solution is

$$\omega(\mathbf{x},t)=\epsilon\sum_{\mathbf{k}_j^c\in\mathcal{P}}(a_j(\tau)\mathbf{w}_j^0(t)+\epsilon^2\mathbf{w}_j^{0,2}(t,\tau)+\cdots)e^{i\mathbf{k}_j^c(t)\cdot\mathbf{x}}+\epsilon^2\sum_{\mathbf{k}_l\in\mathcal{M}}(\mathbf{w}_l^1(t,\tau)+\cdots)e^{i\mathbf{k}_l(t)\cdot\mathbf{x}}+\cdots+\mathrm{c.c.},\tag{11}$$

where $\tau=\epsilon^2 t$ is the slow-time variable, $a_j(\tau)$ are the wave amplitudes, $\mathbf{k}_j^c(t)$ are given by Eq. (9), and the finite sets of wavevectors $\mathcal{P}$ and $\mathcal{M}$ are defined according to initial conditions and nonlinearities. Equation (11) is substituted into Eq. (2) and the terms grouped by each $O(\epsilon^n)$. Then, there are three steps: at $O(\epsilon)$ we determine $\mathbf{w}_j^0(t)$, at $O(\epsilon^2)$ we determine $\mathbf{w}_l^1(t,\tau)$, and at $O(\epsilon^3)$ we impose a nonresonance condition for $\mathbf{w}_j^{0,2}(t,\tau)$, which determines the wave amplitudes $a_j(\tau)$. These steps are detailed below and in Secs. III A and III B, where we first consider a superposition with four waves and then a superposition with an arbitrary number of waves.

The equation for $\mathbf{w}_j^0(t)$ is found from the terms of $O(\epsilon)$. Each $\mathbf{w}_j^0(t)$ satisfies Eq. (6) with ν_c and $\mathbf{k}_j^c(t)$ $(\theta=\theta_c,\ s=s_j)$. Since $\mathbf{k}_j^c$ is a critical wavevector, each $\mathbf{w}_j^0(t)$ may either vanish or become periodic as $t\to+\infty$. For stability, only the periodic case is relevant because the damped Floquet modes are transients and do not affect the long-time behavior. Therefore, we may restrict the initial conditions to a superposition of neutrally stable Floquet modes where Eq. (11) becomes

$$\omega(\mathbf{x},0)=\epsilon\sum_{\mathbf{k}_j^c\in\mathcal{P}}a_j(0)\mathbf{p}_1(-s_j)e^{i\mathbf{k}_j^c(0)\cdot\mathbf{x}}+\mathrm{c.c.},\tag{12}$$

at $t=0$. Then, the solution for each terms of $O(\epsilon)$ is $\mathbf{w}_j^0(t)=\mathbf{p}_1(t-s_j)$.

The set $\mathcal{M}$ in Eq. (11) depends on the nonlinear terms of $O(\epsilon^2)$. The expression for these nonlinear terms involve all possible products of exponentials $e^{\pm i\mathbf{k}_i^c\cdot\mathbf{x}}\cdot e^{\pm i\mathbf{k}_j^c\cdot\mathbf{x}}$ where $\mathbf{k}_i^c$ and $\mathbf{k}_j^c$ belong to $\mathcal{P}$. A *triad* is formed when three wavevectors satisfy $\mathbf{k}_i^c\pm\mathbf{k}_j^c\pm\mathbf{k}_l=0$ and the wavevectors $\mathbf{k}_i^c$ and $\mathbf{k}_j^c\in\mathcal{P}$ are distinct. When $\mathbf{k}_l$ belongs to a triad, then either $\mathbf{k}_l$ or $-\mathbf{k}_l$ must belong to the set $\mathcal{M}$ (the coefficients of $e^{i\mathbf{k}_l\cdot\mathbf{x}}$ and $e^{-i\mathbf{k}_l\cdot\mathbf{x}}$ are complex conjugates of each other).

The set $\mathcal{P}$ in Eq. (11) depends on the initial conditions (12) and on the nonlinear terms of $O(\epsilon^3)$; it contains all $\mathbf{k}_j^c$ such that $a_j(0)\neq 0$ in Eq. (12). Moreover, the set $\mathcal{P}$ also accounts for resonances that occur at $O(\epsilon^3)$. A *four-wave resonance* occurs when four distinct critical wavevectors satisfy $\mathbf{k}_i^c+\mathbf{k}_j^c-\mathbf{k}_m^c-\mathbf{k}_n^c=0$. The set $\mathcal{P}$ must be *closed* with respect to four-wave resonance, i.e., if $\mathbf{k}_i^c$, $\mathbf{k}_j^c$, and $\mathbf{k}_m^c\in\mathcal{P}$, then $\mathbf{k}_n^c\in\mathcal{P}$. To guarantee this property for $\mathcal{P}$, it is sufficient that both wavevectors $\mathbf{k}_j^c$ and $\mathbf{k}_{j'}^c$ belong to $\mathcal{P}$ where $\mathbf{k}_{j'}^c(t)=\mathbf{k}_j^c(t-P/2)$ (the prime over the index denotes half-period displacement).

A. Four-wave resonance

We consider as initial conditions a superposition of plane waves forming a four-wave resonance. Four distinct critical wavevectors $\mathbf{k}_1^c$, $\mathbf{k}_2^c$, $\mathbf{k}_{2'}^c$, and $\mathbf{k}_{1'}^c$,

$$\mathbf{k}_j^c(t)=[\sin\theta_c\cos\Omega(t-s_j),\alpha\sin\theta_c\sin\Omega(t-s_j),\cos\theta_c]^t,\tag{13}$$

form a four-wave resonance, $\mathbf{k}_1^c+\mathbf{k}_{1'}^c-\mathbf{k}_2^c-\mathbf{k}_{2'}^c=0$, only when $s_1=0$, $s_2=s$, $s_{1'}=P/2$, and $s_{2'}=s+P/2$ for some $s\in(0,P/2)$. Notice that $\mathbf{k}_{1'}^c(t)=\mathbf{k}_1^c(t-P/2)$ and $\mathbf{k}_{2'}^c(t)=\mathbf{k}_2^c(t-P/2)$. The initial condition from Eq. (12) is

$$\omega(\mathbf{x},0)=\epsilon(a_1(0)\mathbf{p}_1(-s_1)e^{i\mathbf{k}_1^c(0)\cdot\mathbf{x}}+a_2(0)\mathbf{p}_1(-s_2)e^{i\mathbf{k}_2^c(0)\cdot\mathbf{x}}+a_{1'}(0)\mathbf{p}_1(-s_{1'})e^{i\mathbf{k}_{1'}^c(0)\cdot\mathbf{x}}+a_{2'}(0)\mathbf{p}_1(-s_{2'})e^{i\mathbf{k}_{2'}^c(0)\cdot\mathbf{x}})+\mathrm{c.c.}\tag{14}$$

In Eq. (11), the set $\mathcal{P}$ is $\{\mathbf{k}_1^c,\mathbf{k}_2^c,\mathbf{k}_{1'}^c,\mathbf{k}_{2'}^c\}$ and the set $\mathcal{M}$ has the nine wavevectors $\{\mathbf{k}_3,\mathbf{k}_{3'},\mathbf{k}_4,\mathbf{k}_5,\mathbf{k}_{5'},\mathbf{k}_6,\mathbf{k}_7,\mathbf{k}_8,\mathbf{k}_9\}$, as shown in Table I. This table contains the triads among the wavevectors of $\mathcal{P}$ and $\mathcal{M}$; the upper diagonal gives the sum

Downloaded 17 Nov 2009 to 200.136.239.153. Redistribution subject to AIP license or copyright; see http://pof.aip.org/pof/copyright.jsp

TABLE I. The upper diagonal gives the sum $\mathbf{k}_i^c+\mathbf{k}_j^c$ and the lower diagonal gives the difference $\mathbf{k}_i^c-\mathbf{k}_j^c$.

$\mathbf{k}_i^c \pm \mathbf{k}_j^c$	$\mathbf{k}_1^c$	$\mathbf{k}_2^c$	$\mathbf{k}_{1'}^c$	$\mathbf{k}_{2'}^c$
$\mathbf{k}_1^c$		$-\mathbf{k}_3$	$-\mathbf{k}_9$	$-\mathbf{k}_5$
$\mathbf{k}_2^c$	$\mathbf{k}_4$		$-\mathbf{k}_{5'}$	$-\mathbf{k}_9$
$\mathbf{k}_{1'}^c$	$\mathbf{k}_7$	$\mathbf{k}_6$		$-\mathbf{k}_{3'}$
$\mathbf{k}_{2'}^c$	$\mathbf{k}_6$	$\mathbf{k}_8$	$-\mathbf{k}_4$	

TABLE II. Each nonlinear term $\mathbf{F}_l(t,\tau)$ corresponds to a triad $\mathbf{k}_l \leftarrow \mathbf{k}_i^c \pm \mathbf{k}_j^c$ in Table I and a forcing term in Eq. (18).

$\mathbf{k}_i^c \pm \mathbf{k}_j^c$	$\mathbf{k}_1^c$	$\mathbf{k}_2^c$	$\mathbf{k}_{1'}^c$	$\mathbf{k}_{2'}^c$
$\mathbf{k}_1^c$		$\bar{a}_1\bar{a}_2\mathcal{N}_{12}^+$	0	$\bar{a}_1\bar{a}_{2'}\mathcal{N}_{12'}^+$
$\mathbf{k}_2^c$	$\bar{a}_1 a_2 \mathcal{N}_{12}^-$		$\bar{a}_{1'}\bar{a}_2\mathcal{N}_{1'2}^+$	0
$\mathbf{k}_{1'}^c$	$\bar{a}_1 a_{1'}\mathcal{N}_{11'}^-$	$a_{1'}\bar{a}_2\mathcal{N}_{1'2}^-$		$\bar{a}_{1'}\bar{a}_{2'}\mathcal{N}_{1'2'}^+$
$\mathbf{k}_{2'}^c$	$\bar{a}_1 a_{2'}\mathcal{N}_{12'}^-$	$\bar{a}_2 a_{2'}\mathcal{N}_{22'}^-$	$a_{1'}\bar{a}_{2'}\mathcal{N}_{1'2'}^-$	

$\mathbf{k}_i^c+\mathbf{k}_j^c$, while the lower diagonal gives the difference $\mathbf{k}_i^c-\mathbf{k}_j^c$, where i is the index of the line and j the index of the column. There are three wavevectors that belong to two different triads: $\mathbf{k}_4$, $\mathbf{k}_6$, and $\mathbf{k}_9$. A representation of the sets $\mathcal{P}$ and $\mathcal{M}$ in the xy-plane is given in Fig. 2 where vectors with solid lines indicate wavevectors in $\mathcal{P}$ and vectors with dashed lines indicate wavevectors in $\mathcal{M}$.

For the terms of $O(\epsilon)$ the solutions are $\mathbf{w}_1^0(t)=\mathbf{p}_1(t-s_1)$, $\mathbf{w}_2^0(t)=\mathbf{p}_1(t-s_2)$, $\mathbf{w}_{1'}^0(t)=\mathbf{p}_1(t-s_{1'})$, and $\mathbf{w}_{2'}^0(t)=\mathbf{p}_1(t-s_{2'})$. Each $\mathbf{w}_j^0(t)$ corresponds to a velocity vector $\mathbf{v}_j^0=i\mathbf{k}_j^c \times \mathbf{w}_j^0/\|\mathbf{k}_j\|^2$, $j=1,2,1',2'$. For the terms of $O(\epsilon^2)$, each $\mathbf{w}_l^1(t,\tau)$ must satisfy the equation

$$\dot{\mathbf{w}}_l^1 + \mathcal{L}(\mathbf{k}_l)\mathbf{w}_l^1 + \nu_c\|\mathbf{k}_l\|^2\mathbf{w}_l^1 = \mathbf{F}_l(t,\tau), \tag{15}$$

where $\mathbf{k}_l \in \mathcal{M}$, and $\mathbf{F}_l(t,\tau)$ is formed by products of terms of $O(\epsilon)$. Each product can be identified with a triad and each triad can be denoted as $\mathbf{k}_l \leftarrow \mathbf{k}_i^c \pm \mathbf{k}_j^c$ when either $\mathbf{k}_l=\mathbf{k}_i^c \pm \mathbf{k}_j^c$ or $\mathbf{k}_l=-(\mathbf{k}_i^c \pm \mathbf{k}_j^c)$. To the triads $\mathbf{k}_l \leftarrow \mathbf{k}_i^c+\mathbf{k}_j^c$ (upper diagonal of Table I) we associate the function

$$\begin{aligned}\mathcal{N}_{ij}^+(t) = i[&(\mathbf{k}_i^c\cdot\mathbf{w}_j^0)\mathbf{v}_i^0 + (\mathbf{k}_j^c\cdot\mathbf{w}_i^0)\mathbf{v}_j^0 \\ &- (\mathbf{k}_i^c\cdot\mathbf{v}_j^0)\mathbf{w}_i^0 - (\mathbf{k}_j^c\cdot\mathbf{v}_i^0)\mathbf{w}_j^0],\end{aligned} \tag{16}$$

and to the triads $\mathbf{k}_l \leftarrow \mathbf{k}_i^c-\mathbf{k}_j^c$ (lower diagonal of Table I) we associate the function

$$\begin{aligned}\mathcal{N}_{ij}^-(t) = i[&(\mathbf{k}_i^c\cdot\mathbf{w}_j^0)\mathbf{v}_i^0 + (\mathbf{k}_j^c\cdot\mathbf{w}_i^0)\mathbf{v}_j^0 \\ &+ (\mathbf{k}_i^c\cdot\mathbf{v}_j^0)\mathbf{w}_i^0 + (\mathbf{k}_j^c\cdot\mathbf{v}_i^0)\mathbf{w}_j^0].\end{aligned} \tag{17}$$

The divergence-free condition implies $\mathcal{N}_{jj}^{\pm}(t)=0$ and in Appendix A we prove that $\mathcal{N}_{jj'}^+(t)=0$. Each triad $\mathbf{k}_l \leftarrow \mathbf{k}_i^c \pm \mathbf{k}_j^c$ in Table I corresponds to one term in the right-hand side of Eq. (15) given in Table II. For example, $\mathbf{F}_3(t,\tau)=\bar{a}_1\bar{a}_2\mathcal{N}_{12}^+$, $\mathbf{F}_4(t,\tau)=\bar{a}_1 a_2\mathcal{N}_{12}^- + a_{1'}\bar{a}_{2'}\mathcal{N}_{1'2'}^-$, and $\mathbf{F}_9(t,\tau)=0$. The dependence of $\mathbf{F}_l(t,\tau)$ on τ is explicit, so that to solve Eq. (15), it remains to find the solution of

$$\dot{\mathbf{w}}_{ij}^{\pm} + \mathcal{L}(\mathbf{k}_l)\mathbf{w}_{ij}^{\pm} + \nu_c\|\mathbf{k}_l\|^2\mathbf{w}_{ij}^{\pm} = \mathcal{N}_{ij}^{\pm}(t) \tag{18}$$

for each term $\mathcal{N}_{ij}^{\pm}(t)$ that appears in Table II. The solutions $\mathbf{w}_{ij}^{\pm}(t)$ eventually become periodic because $\mathcal{N}_{ij}^{\pm}(t)$ is periodic and the homogeneous Eq. (18) has asymptotically stable solutions. We are only interested in the periodic solutions since transient decay is not important for long-time stability. The appropriate initial condition to obtain the periodic solution of Eq. (15) is

$$\mathbf{w}_{ij}^{\pm}(0) = (\mathbf{I}-\mathbf{X}_l(P))^{-1}\mathbf{X}_l(P)\int_0^P \mathbf{X}_l^{-1}(s)\mathcal{N}_{ij}^{\pm}(s)ds, \tag{19}$$

where $\mathbf{X}_l(t)$ is the fundamental matrix of the homogeneous equation (the inverse of $\mathbf{I}-\mathbf{X}_l(P)$ always exists). Numerical integration is used to compute the $\mathbf{w}_{ij}^{\pm}(t)$ with Eq. (19). Once the periodic solutions of Eq. (18) are known, the solutions of Eq. (15) are given by

$$\begin{aligned}
&\mathbf{w}_3^1(t,\tau) = \bar{a}_1(\tau)\bar{a}_2(\tau)\mathbf{w}_{12}^+(t),\\
&\mathbf{w}_{3'}^1(t,\tau) = \bar{a}_{1'}(\tau)\bar{a}_{2'}(\tau)\mathbf{w}_{1'2'}^+(t),\\
&\mathbf{w}_5^1(t,\tau) = \bar{a}_1(\tau)\bar{a}_{2'}(\tau)\mathbf{w}_{12'}^+(t),\\
&\mathbf{w}_{5'}^1(t,\tau) = \bar{a}_{1'}(\tau)\bar{a}_2(\tau)\mathbf{w}_{1'2}^+(t),\\
&\mathbf{w}_7^1(t,\tau) = \bar{a}_1(\tau)a_{1'}(\tau)\mathbf{w}_{11'}^-(t),\\
&\mathbf{w}_8^1(t,\tau) = \bar{a}_2(\tau)a_{2'}(\tau)\mathbf{w}_{22'}^-(t),\\
&\mathbf{w}_4^1(t,\tau) = \bar{a}_1(\tau)a_2(\tau)\mathbf{w}_{12}^-(t) + a_{1'}(\tau)\bar{a}_{2'}(\tau)\mathbf{w}_{1'2'}^-(t),\\
&\mathbf{w}_6^1(t,\tau) = \bar{a}_1(\tau)a_{2'}(\tau)\mathbf{w}_{12'}^-(t) + a_{1'}(\tau)\bar{a}_2(\tau)\mathbf{w}_{1'2}^-(t),\\
&\mathbf{w}_9^1(t,\tau) = 0.
\end{aligned} \tag{20}$$

Notice that the average damping $(\nu_c/P)\int_0^P\|\mathbf{k}_l\|^2dt$ in Eq. (15) must not vanish as $\epsilon\to 0$; otherwise Ansatz (11) does not hold. As the average damping decreases, the size of the solution of Eq. (15) increases in the inverse proportion and if the average damping becomes of order ϵ, the ordering of the terms in the Ansatz is violated. Therefore, we must restrict the analysis to cases where neither ν_c nor $\|\mathbf{k}_l\|$ is small. The viscosity ν_c vanishes along the neutral curve either in the $\beta\to 0$ limit or in the $\beta\to 1$ limit, which are the special cases

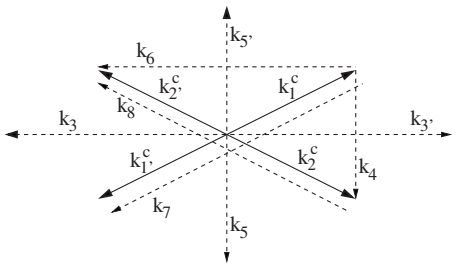


FIG. 2. Schematic representation of wavevector projection in the xy-plane. The wavevectors belonging to $\mathcal{P}$ and $\mathcal{M}$ are marked with solid and dashed lines, respectively. The wavevectors $\mathbf{k}_3$, $\mathbf{k}_{3'}$, $\mathbf{k}_5$, and $\mathbf{k}_{5'}$ have the z-component equal to $2\cos\theta_c$. The wavevector $\mathbf{k}_9=(0,0,2\cos\theta_c)$.

Downloaded 17 Nov 2009 to 200.136.239.153. Redistribution subject to AIP license or copyright; see http://pof.aip.org/pof/copyright.jsp

of a circular flow and a shear flow, respectively. A wavevector $\|\mathbf{k}_l\|$ tends to zero in either the limits $s \to 0$ or $s \to P/2$ because these limits imply that either $\|\mathbf{k}_4\| \to 0$ or $\|\mathbf{k}_6\| \to 0$. The balance between the viscous term and the forcing term of Eq. (15) shows that $\|\mathbf{w}_4\|$ scale with s^{-1} as $s \to 0$, and the equivalent happens with $\|\mathbf{w}_6\|$ as $s \to P/2$. We restrict our analysis to the case where $\|\mathbf{k}_4\|$ and $\|\mathbf{k}_6\|$ are of order one, but modifying the asymptotic Ansatz could allow other scalings for $\|\mathbf{k}_4\|$ or $\|\mathbf{k}_6\|$.

Next, we proceed to the terms of $O(\epsilon^3)$, where the equation for $\mathbf{w}_n^{0,2}(t,\tau)$ is

$$\dot{\mathbf{w}}_n^{0,2} + \mathcal{L}(\mathbf{k}_n^c)\mathbf{w}_n^{0,2} + \nu_c\|\mathbf{k}_n^c\|^2\mathbf{w}_n^{0,2} = -\frac{da_n}{d\tau}\mathbf{w}_n^0(t) - \nu_2\|\mathbf{k}_n\|^2 a_n \mathbf{w}_n^0(t) + \mathbf{G}_n(t,\tau), \tag{21}$$

where $\mathbf{k}_n^c \in \mathcal{P}$ and the perturbed viscosity is $\nu = \nu_c + \epsilon^2\nu_2$. The right-hand side has three terms: the first is the slow-time differentiation of the wave amplitudes, the second is the perturbation of the critical viscosity, and the third is the nonlinear *feedback*. In the feedback terms we use the following notations:

$$\mathcal{N}_{mij}^{++}(t) = i[(\mathbf{k}_m^c \cdot \mathbf{w}_{ij}^{\pm})\mathbf{v}_m^0 + (\mathbf{k}_l \cdot \mathbf{w}_m^0)\mathbf{v}_{ij}^{\pm} - (\mathbf{k}_m^c \cdot \mathbf{v}_{ij}^{\pm})\mathbf{w}_m^0 - (\mathbf{k}_l \cdot \mathbf{v}_m^0)\mathbf{w}_{ij}^{\pm}], \tag{22}$$

$$\mathcal{N}_{mij}^{--}(t) = i[(\mathbf{k}_m^c \cdot \mathbf{w}_{ij}^{\pm})\mathbf{v}_m^0 + (\mathbf{k}_l \cdot \mathbf{w}_m^0)\mathbf{v}_{ij}^{\pm} + (\mathbf{k}_m^c \cdot \mathbf{v}_{ij}^{\pm})\mathbf{w}_m^0 + (\mathbf{k}_l \cdot \mathbf{v}_m^0)\mathbf{w}_{ij}^{\pm}], \tag{23}$$

where $\mathbf{w}_{ij}^{\pm}$ is the solution of Eq. (18) and the velocity vector is $\mathbf{v}_{ij}^{\pm} = i\mathbf{k}_l \times \mathbf{w}_{ij}^{\pm}/\|\mathbf{k}_l\|^2$. The nonlinear terms $\mathcal{N}_{mij}^{++}(t)$ or $\mathcal{N}_{mij}^{--}(t)$ appear in the feedback $\mathbf{G}_n(t,\tau)$ when $\mathbf{k}_n^c \leftarrow \mathbf{k}_m^c \pm \mathbf{k}_l$ for $\mathbf{k}_m^c \in \mathcal{P}$ and $\mathbf{k}_l \in \mathcal{M}$, where $\mathbf{k}_l \leftarrow \mathbf{k}_i^c \pm \mathbf{k}_j^c$ for a pair of wavevectors $\mathbf{k}_i^c$ and $\mathbf{k}_j^c \in \mathcal{P}$. Using the above expressions, the feedback terms can be written as

$$\mathbf{G}_1(t,\tau) = a_1|a_2|^2(\mathcal{N}_{212}^{++} + \mathcal{N}_{212}^{--}) + a_1|a_{2'}|^2(\mathcal{N}_{2'12'}^{++} + \mathcal{N}_{2'12'}^{--}) + a_2\bar{a}_{1'}a_{2'}(\mathcal{N}_{21'2'}^{--} + \mathcal{N}_{2'1'2}^{--}) + a_1|a_{1'}|^2\mathcal{N}_{1'11'}^{--}, \tag{24}$$

$$\mathbf{G}_2(t,\tau) = a_2|a_1|^2(\mathcal{N}_{112}^{++} + \mathcal{N}_{112}^{+-}) + a_1a_{1'}\bar{a}_{2'}(\mathcal{N}_{11'2'}^{+-} + \mathcal{N}_{1'12'}^{--}) + a_2|a_{1'}|^2(\mathcal{N}_{1'1'2}^{--} + \mathcal{N}_{1'1'2}^{++}) + a_2|a_{2'}|^2\mathcal{N}_{2'22'}^{--}, \tag{25}$$

and similar expressions hold for $\mathbf{G}_{1'}(t,\tau)$ and $\mathbf{G}_{2'}(t,\tau)$. The functions $\mathbf{G}_n(t,\tau)$ are periodic in t. To avoid a resonant solution for $\mathbf{w}_n^{0,2}$, the right-hand side of Eq. (21) must be orthogonal to the periodic solution of

$$-\dot{\mathbf{q}}_n + \mathcal{L}^t(\mathbf{k}_n)\mathbf{q}_n + \nu_c\|\mathbf{k}_n\|^2\mathbf{q}_n = 0, \tag{26}$$

where $\mathcal{L}^t$ is the transpose of $\mathcal{L}$ and the scalar product of $\mathbf{p}(t)$ and $\mathbf{q}(t)$ is defined as

$$(\mathbf{q},\mathbf{p}) = \frac{1}{P}\int_0^P \bar{\mathbf{q}}^t\mathbf{p}\,dt. \tag{27}$$

Since a Floquet exponent is zero, Eq. (26) has a real periodic solution $\mathbf{q}_n(t)$ where each $\mathbf{q}_n(t)$ is a time displacement of $\mathbf{q}_1(t)$: $\mathbf{q}_n(t) = \mathbf{q}_1(t - s_n)$ and $n = 1, 2, 1', 2'$. The initial value $\mathbf{q}_1(0)$ is normalized so that $\mathbf{q}_1^t(0)\mathbf{p}_1(0) = 1$, from which it follows that $(\mathbf{q}_n, \mathbf{w}_n^0) = 1$.

Taking the scalar product of $\mathbf{q}_n(t)$, $n = 1, 2, 1', 2'$, with the right-hand side of Eq. (21) and equating it to zero yields the following four scalar equations for the wave amplitudes:

$$\frac{da_1}{d\tau} = -\kappa a_1 + a_1(c_{12}|a_2|^2 + c_{11'}|a_{1'}|^2 + c_{12'}|a_{2'}|^2) + c_{11}\bar{a}_{1'}a_2a_{2'}, \tag{28}$$

$$\frac{da_2}{d\tau} = -\kappa a_2 + a_2(c_{21}|a_1|^2 + c_{22'}|a_{2'}|^2 + c_{21'}|a_{1'}|^2) + c_{22}\bar{a}_{2'}a_1a_{1'}, \tag{29}$$

$$\frac{da_{1'}}{d\tau} = -\kappa a_{1'} + a_{1'}(c_{12}|a_{2'}|^2 + c_{11'}|a_1|^2 + c_{12'}|a_2|^2) + c_{11}\bar{a}_1a_{2'}a_2, \tag{30}$$

$$\frac{da_{2'}}{d\tau} = -\kappa a_{2'} + a_{2'}(c_{21}|a_{1'}|^2 + c_{22'}|a_2|^2 + c_{21'}|a_1|^2) + c_{22}\bar{a}_2a_{1'}a_1, \tag{31}$$

where the coefficients are

$$\begin{aligned} &c_{12} = (\mathbf{q}_1, \mathcal{N}_{212}^{++} + \mathcal{N}_{212}^{--}), \quad c_{11'} = c_{22'} = (\mathbf{q}_1, \mathcal{N}_{1'11'}^{--}), \\ &c_{12'} = (\mathbf{q}_1, \mathcal{N}_{2'12'}^{++} + \mathcal{N}_{2'12'}^{--}), \quad c_{11} = (\mathbf{q}_1, \mathcal{N}_{21'2'}^{--} + \mathcal{N}_{2'1'2}^{--}), \\ &c_{21} = (\mathbf{q}_2, \mathcal{N}_{112}^{++} + \mathcal{N}_{112}^{+-}), \quad c_{21'} = (\mathbf{q}_2, \mathcal{N}_{1'1'2}^{--} + \mathcal{N}_{1'1'2}^{++}), \\ &c_{22} = (\mathbf{q}_2, \mathcal{N}_{11'2'}^{+-} + \mathcal{N}_{1'12'}^{--}), \end{aligned} \tag{32}$$

and $\kappa = \nu_2\int_0^P \|\mathbf{k}_n(t)\|^2 dt = \nu_2(1 + \alpha^2 \sin^2\theta_c)/2$. The above system is invariant under the exchange of index $a_j \leftrightarrow a_{j'}$ because the initial condition (12) is also invariant under the same exchange of index followed by a half-period displacement, $t \to t - P/2$. The above system could be obtained *a priori* using symmetry arguments[17] but, of course, without the numerical values of the coefficients. The coefficients depend on s and we compute them using numerical integration for $s = jP/256$ for $j = 1, \ldots, 127$. Notice that some coefficients scale with s^{-1} as $s \to 0$ while some other coefficients scale with $(s - P/2)^{-1}$ as $s \to P/2$ [a consequence of the vanishing damping in Eq. (15)]. In the following we use these scalings to find the largest coefficients but avoid the limiting cases that would require a different Ansatz for the asymptotic solution.

B. Superpositions of many waves

Here we derive the ODE for the wave amplitudes when there are many plane waves superposed. We consider the special case of a superposition of $2n$ plane waves with wavevectors equally spaced in time. In Eq. (11), the set $\mathcal{P}$ consists of all $\mathbf{k}_j^c$ given by Eq. (13) with $s_j = j\Delta T$, for $j = 0, \ldots, 2n-1$, and $\Delta T = P/(2n)$, so that $\mathcal{P}$ is closed with re-

Downloaded 17 Nov 2009 to 200.136.239.153. Redistribution subject to AIP license or copyright; see http://pof.aip.org/pof/copyright.jsp

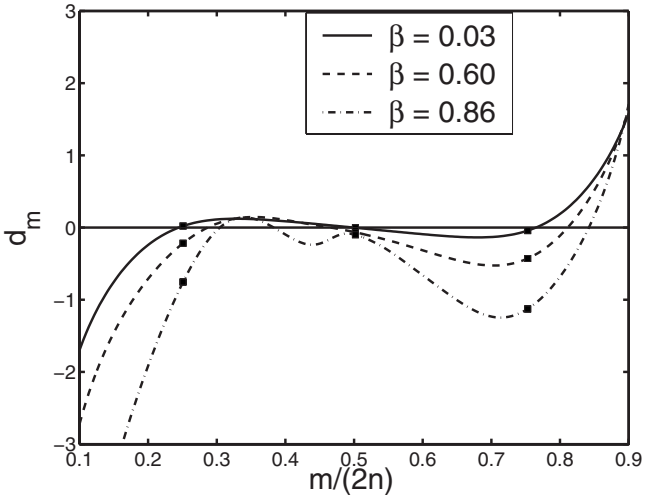


FIG. 3. d_m vs $m/(2n)$ for $m=1,\ldots,2n-1$. The three lines (solid, dashed, and dash-dotted) join the values of d_m for $n=128$ for three values of β (legend). The squares indicate the values of d_m when $n=2$ for the same three values of β. For $n\geq 4$, the extreme values of d_m occur at $d_1<0$ and $d_{2n-1}>0$. For $n=2$, $d_1>0$ and $d_3<0$ when $\beta<0.14$, while $d_1\leq 0$ and $d_3<0$ when $\beta\geq 0.14$.

spect to four-wave resonances. To simplify the notation, we allow the index j to be periodic, $j\equiv j(\mathrm{mod}\ 2n)$, and we use a prime to denote addition by n to the index, i.e., $a_{j'}\equiv a_{j+n}$ and $\mathbf{k}^c_{j'}\equiv\mathbf{k}^c_{j+n}$. Next, we show that the ODE for the wave amplitudes must have the form

$$\frac{da_j}{d\tau}=-\kappa a_j+a_j\sum_{i=0}^{2n-1}d_{i-j}|a_i|^2+\bar{a}_{j'}\sum_{i=0}^{n-1}h_{i-j}a_ia_{i'}, \tag{33}$$

for $j=0,\ldots,2n-1$, where d_m is a vector with periodic index $m\equiv m(\mathrm{mod}\ 2n)$ and h_l is a vector with periodic index $l\equiv l(\mathrm{mod}\ n)$. In Eq. (33), the cubic term $a_j|a_i|^2$ is associated with the triads $\mathbf{k}^c_j\pm\mathbf{k}^c_i\pm\mathbf{k}_l=0$, while the cubic term $\bar{a}_{j'}a_ia_{i'}$ is associated with the four-wave resonances $\mathbf{k}^c_j+\mathbf{k}^c_{j'}-\mathbf{k}^c_i-\mathbf{k}^c_{i'}=0$. The coefficients of these nonlinear terms must be such that Eq. (33) is invariant under either one of the maps: (i) $a_j\to a_{j+1}$ or (ii) $a_j\to a_{j'}$. These restrictions follow from the invariance of Eq. (11) under either map (i) followed by the time shift $t\to t+\Delta T$ or map (ii) followed by the half-period displacement $t\to t-P/2$. To determine the numerical values of d_m and h_l, we observe that Eq. (33) reduces to Eqs. (28)–(31) when Eq. (33) has only four nonzero components $a_0(\tau)$, $a_i(\tau)$, $a_{0'}(\tau)$, and $a_{i'}(\tau)$, and Eq. (13) has $s=i\Delta T$. By comparing both equations, we find that d_m and h_l can be determined from Eq. (32), such that $d_i=c_{12}$, $d_{n-i}=c_{21'}$, $d_n=c_{11'}$, $d_{n+i}=c_{12'}$, $d_{2n-i}=c_{21}$, $h_i=c_{11}$, and $h_{n-i}=c_{22}$ for $i=1\ldots\lfloor n/2\rfloor$. In particular, $d_0=0$ and $h_0=0$ because only distinct wavevectors can form triads and four-wave resonances. Figure 3 shows the vector d_m for different values of β and n. For large n, $|d_1|$ and $d_{-1}\equiv d_{2n-1}$ grow linearly with n, which occurs because these coefficients scale with s^{-1} in Eqs. (28)–(31). The coefficients h_1 and h_{-1} are the largest coefficients of h_l in absolute value and they also scale with s^{-1} ($h_1<0$ and $h_{-1}>0$).

Equation (33) can be written in a vectorial form $d\mathbf{a}/d\tau=-\kappa\mathbf{a}+\mathcal{Q}(\mathbf{a})$ where $\mathbf{a}(\tau)$ is the solution vector, $\mathbf{a}(\tau)=[a_0,a_1,\ldots,a_{2n-1}]^t$, and $\mathcal{Q}(\mathbf{a})$ denotes the cubic term. We rescale Eq. (33) in its vectorial form using $\tau=BT$, $\mathbf{a}(\tau)=M\mathbf{y}(T)$, and $\mathcal{Q}(\cdot)=Q\mathbf{Q}(\cdot)$, where B, M, and Q, are positive constants. This yields the system

$$\frac{d\mathbf{y}}{dT}=-\xi\mathbf{y}+\mathbf{Q}(\mathbf{y}), \tag{34}$$

with $B=M^{-2}Q^{-1}$ and $\xi=\kappa M^{-2}Q^{-1}$. The rescaling factor M in Eq. (34) is chosen so that $\|\mathbf{y}(0)\|_\infty=1$ and Q is chosen so that the absolute value of the largest coefficient of $\mathbf{Q}(\cdot)$ is one; the rescaled coefficients are denoted with capital letters $D_m=d_m/Q$ and $H_l=h_l/Q$.

IV. WEAKLY NONLINEAR STABILITY

Here we study Eq. (34) regarding (i) the stability of a CCW, (ii) the bifurcation occurring at $\xi=0$, and (iii) the global stability. (i) A CCW corresponds to a solution of Eq. (34) where $y_0(T)=Ke^{-\xi T}$ and $y_j(T)=0$ for $j\neq 0$; exponential growth occurs when $\xi<0$. The exponentially growing solution is stable if the trajectories of Eq. (34) approach the y_0-plane (complex plane) when initially $|y_0(0)|=1$ and the components $y_j(0)$, $j\neq 0$, are sufficiently small. To study stability, the quadratic and cubic terms in y_j, $j\neq 0$, can be initially neglected and Eq. (34) reduces to

$$\frac{dy_0}{dT}=-\xi y_0, \tag{35}$$

$$\frac{dy_j}{dT}=(-\xi+D_{-j}|y_0|^2)y_j, \tag{36}$$

for $1\leq j\leq 2n-1$. The component y_0 grows exponentially; therefore, the solution trajectory approaches the y_0-plane if, and only if, $D_j<0$ for all $j\neq 0$ (otherwise one of the y_j eventually grows). In general, a CCW is unstable since for every β and $n\geq 4$ there is always a positive value of D_m as seen in Fig. 3. Next we show that, for $n\geq 4$, the instability of y_0 leads to the growth of component y_1 which, in turn, suppresses the growth of y_0. Since the largest value of D_m occurs at $D_{-1}>0$ ($D_{-1}\equiv D_{2n-1}$ in Fig. 3), this suggests that the most unstable component of $\mathbf{y}$ is y_1 as seen from Eq. (36). Thus, once $y_1(T)$ becomes relatively large, and assuming the other components y_j remain small, Eq. (34) can be approximated by a two-component system,

$$\frac{dy_0}{dT}=(-\xi+D_1|y_1|^2)y_0, \tag{37}$$

$$\frac{dy_1}{dT}=(-\xi+D_{-1}|y_0|^2)y_1. \tag{38}$$

If this approximation remains valid, $y_0(T)$ decreases fast after it reaches its maximum because $D_1<0$ is the smallest component of D_m. Thus, the growth of component y_1 causes y_0 to be damped. The above analysis is also valid for any pair of components y_j and y_{j+1} because Eq. (34) is invariant under the map $y_j\to y_{j+1}$. Thus, component y_j promotes the growth of y_{j+1} which promotes the decay of y_j, i.e., there is a cycle of growth and decay and the cycle moves from component y_j

Downloaded 17 Nov 2009 to 200.136.239.153. Redistribution subject to AIP license or copyright; see http://pof.aip.org/pof/copyright.jsp

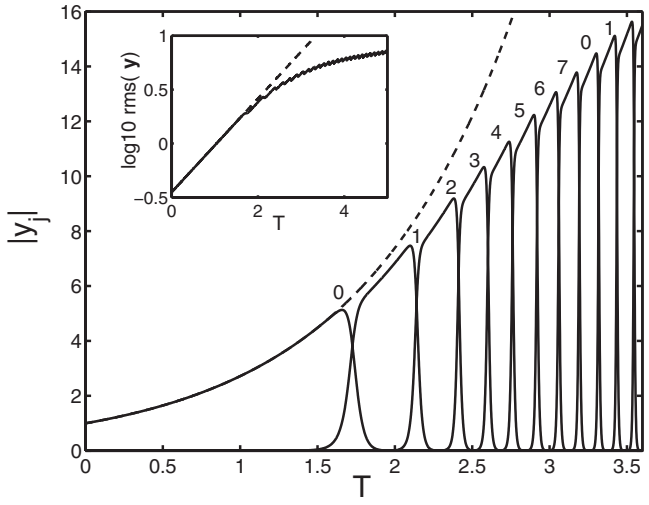


FIG. 4. Instability of a CCW for $n=4$, $\beta=0.2$, $\xi=-1$, $T\in[0,3.6]$. The initial condition is $y_0(0)=1$ and $y_i(0)$ is random for $1\le i\le 7$ with $|y_i(0)|\le 10^{-5}$. Each line represents one component $y_i(T)$, indicated by the number close to its peak. The dashed lines indicate the exponential e^T (growth of a CCW). Initially, y_0 grows exponentially fast. This growth is interrupted by the growth of y_1. Cycles of growth and decay occur in a succession from y_j to y_{j+1}. Each cycle has a higher peak and a shorter period. The solution has a subexponential growth; the inset shows $\log_{10}\mathrm{rms}(\mathbf{y}(T))$ with $T\in[0,5]$ where $\mathrm{rms}(\mathbf{y})=\sqrt{\Sigma_{j=0}^{2n-1}y_j/(2n)}$.

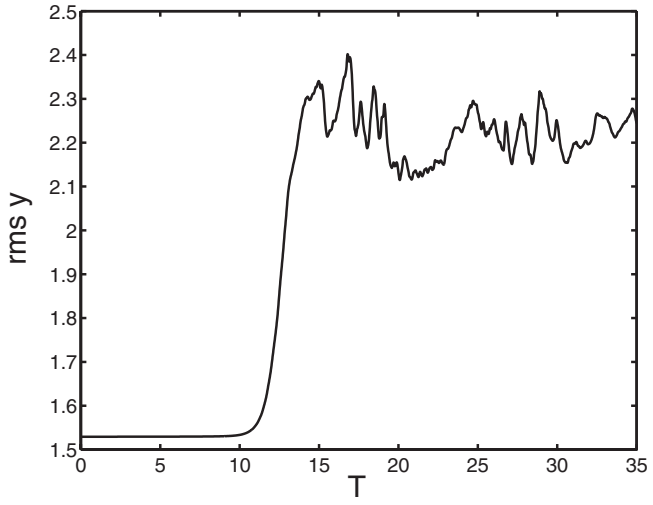


FIG. 5. Saturation of wave amplitudes with $n=8$, $\xi=-1$, and $\beta=0.2$. The vertical axis is $\mathrm{rms}(\mathbf{y}(T))$ with $T\in[0,35]$. The initial condition is a critical point plus a random perturbation of magnitude 10^{-5}. After a transient period, the solution develops chaotic oscillations within well defined bounds.

to y_{j+1}. A numerical calculation showing the growth-and-decay cycle is given in Fig. 4 and a detailed account of the numerical procedure is given in Appendix B. Initially, y_0 grows exponentially fast, this growth being interrupted smoothly by the growth of y_1. Growth-and-decay cycles occur in a succession, each cycle having a higher peak and a shorter period. The peaks are lower than the exponential growth of an undisturbed CCW. The same behavior is observed for other values of β and $n\ge 4$. For $n=2$, the CCW is unstable for $\beta<0.14$ and stable for $\beta\ge 0.14$. For $\beta<0.14$, $D_1>0$ is the only positive value of D_m (the square marks on the solid line in Fig. 3). The sign of D_1 changes for $\beta\ge 0.14$ and the CCW becomes stable. For $n=1$, the CCW is also stable since it is a special case of Eqs. (42) and (43) discussed below.

(ii) A bifurcation occurs in Eq. (34) when the parameter ξ changes sign. For $\xi>0$, the origin is a local asymptotically stable point and it becomes unstable when $\xi<0$. In the subspace where $a_j(\tau)=a(\tau)$ for every j, Eq. (34) reduces to

$$\frac{da}{d\tau}=(-\xi+\lambda|a|^2)a, \tag{39}$$

where λ is the Landau constant given by

$$\lambda=\sum_{m=0}^{2n-1}D_m+\sum_{l=0}^{n-1}H_l. \tag{40}$$

The bifurcation is always supercritical since λ is negative for all values of β and n; furthermore, λ decreases as β increases. The contribution of triads and four-wave resonances are stabilizing since both sums in D_m and H_l are negative and have the same order of magnitude. The critical points of Eq. (34) that bifurcate form the origin when $\xi<0$ are given by

$$Y_j=e^{i\psi_j}\sqrt{\xi/\lambda}, \tag{41}$$

where the angles ψ_j satisfy $\psi_j+\psi_{j'}=\psi^*$ with a common ψ^* for all j; in total, there are $n+1$ free parameters. The critical points Y_j are unstable, and the trajectories starting near Y_j eventually lead to a chaotic behavior within well defined bounds as illustrated in Fig. 5. After a period of transition, the solution develops chaotic oscillations within well defined bounds. Similar qualitative behavior is found for other values of n and β.

(iii) Another aspect of Eq. (34) is its global stability. The existence of a finite-time blowup would imply the existence of a fast transition. For general initial conditions, simulations were performed with random initial data for different values of n and β. For $\xi<0$, we find that the wave amplitudes oscillate chaotically within well defined bounds after a brief period of adjustment; while for $\xi>0$, the wave amplitudes decay to zero. Thus, there is no evidence of a finite-time blowup for a typical initial condition (we have tested several randomly chosen initial conditions). Next, we investigate if a particular triad can lead to a finite-time blowup. Consider Eq. (34) with two nonzero components $y_0(t)$ and $y_i(t)$, where $y_j=0$ for $j\ne 0$ and $j\ne i$. Equation (34) reduces to

$$\frac{dy_0}{dT}=-\xi y_0+D_i y_0|y_i|^2, \tag{42}$$

$$\frac{dy_i}{dT}=-\xi y_i+D_{-i}|y_0|^2 y_i, \tag{43}$$

where the coefficients D_i and D_{-i} depend on β. It can be shown that a finite-time blowup exists if, and only if, both coefficients D_i and D_{-i} are positive. Inspection of the values of D_i and D_{-i} over all values of β and $i=1,\cdots,n$, with $n=128$, reveals that they are never both positive. The solution of Eqs. (42) and (43) converges to zero when $\xi>0$ and it converges to a CCW when $\xi<0$. Lastly, we investigate if a particular symmetry of a four-wave resonance of Eq. (34)

Downloaded 17 Nov 2009 to 200.136.239.153. Redistribution subject to AIP license or copyright; see http://pof.aip.org/pof/copyright.jsp

can lead to a finite-time blowup. We consider four-wave amplitudes with half-period conjugate symmetry, i.e., $y_0=\bar{y}_{0'}$, $y_i=\bar{y}_{i'}$, and $y_j=0$ for $j\neq 0,0',i,i'$. The change in variables $x_1=|y_0|^2$ and $x_j=|y_j|^2$ yields the system

$$\frac{1}{2}\frac{dx_1}{d\tau}+\xi x_1=\alpha x_1x_2+Cx_1^2, \tag{44}$$

$$\frac{1}{2}\frac{dx_2}{d\tau}+\xi x_2=\alpha' x_1x_2+Cx_2^2. \tag{45}$$

For the whole range of parameters n, i, and β, the value of C is always negative while the values of α and α' are never positive simultaneously. In this case, it can be shown that the solution of Eqs. (44) and (45) always converges to a critical point [in particular when ξ, α, and α' are negative, Eqs. (44) and (45) are classical competition models for two species[18]].

V. DISCUSSIONS AND CONCLUSION

Our weakly nonlinear asymptotics described the disturbance of the elliptical flow as a superposition of plane waves with slowly evolving amplitudes. We derived an ODE for the slow-time evolution of the wave amplitudes at cubic order, Eq. (34), valid when the eccentricity of the streamlines is neither one nor infinity. The neutral curve used in the analysis has been reported by Landman and Saffman[5] and summarized here for completion (Fig. 1). For subcritical ν, our numerical calculations show that the wave amplitudes eventually vanish. For supercritical ν, our analysis suggests that short-wave elliptical instability is likely to saturate but there are exceptions. For generic initial conditions our numerical calculations showed that the wave amplitudes saturate in a chaotic state, and we have not found evidence of a finite-time blowup at cubic order. Still, we cannot conclude that the bifurcation at the neutral curve is supercritical because there are solutions that do not saturate. For example, a single CCW is an exact solution of the NSE for our model flow and the exponential growth in the supercritical region continues regardless of its amplitude. Moreover, when a CCW is perturbed, the solution shows growth-and-decay cycles among the wave amplitudes (Fig. 4). Since successive cycles occur between neighboring CCWs, the superpositions may still resemble a CCW when, in fact, the dominant wave amplitude changes from one CCW to another. Moreover, the weakly nonlinear effects are stabilizing since the solution of Eq. (34) has a subexponential growth rate (Fig. 4).

The saturation of mode amplitudes has been found by weakly nonlinear analysis in the rotating elliptical tank by Waleffe[19] and in the strained Lamb–Oseen vortex by Sipp.[20] Although our analysis shows saturation of wave amplitudes for generic initial conditions, we also find a nonsaturated dynamics incompatible with a genuine supercritical bifurcation. In particular, the nonsaturated dynamics are linked to the exponential growth of a single CCW. The exponential growth persists because the nonlinear interaction of a CCW with itself is null and, therefore, it does not generate a mean-flow correction. In this respect, the studies of Waleffe and Sipp included mean-flow interactions by considering the global modes and found saturation. A shortcoming of our model flow is that it ignores the length scale for matching the local flow with the global flow. There is a maximum length scale L where the streamlines of the global flow can be regarded as elliptic and far from boundaries. For this reason, in the model flow, the wavelengths of the CCWs should be much smaller than L and we need to limit the length of the longest wave in our analysis. According to our local mode approximation, we kept only nonlinear interactions among short-wave modes and excluded interactions of short wavelengths with long wavelengths. Mathematically, this is expressed by avoiding the limits $\|\mathbf{k}_4\|\to 0$ and $\|\mathbf{k}_6\|\to 0$ in Eq. (15).

We are assuming that mean-flow corrections would be of a higher order, so that solutions that do not saturate at cubic order could do so at a higher order. This is seen by interpreting our analysis as a special case of a geometrical-optics multiphase solution, as follows. Let us consider a global-flow $\mathbf{U}_0(x,y)$ with elliptical streamlines within a radius R from the origin. Consider a perturbation $\mathbf{u}(\mathbf{x},t)$ with asymptotic solution

$$\mathbf{u}(\mathbf{x},t)=\sum_j(\epsilon\mathbf{A}_{j1}(\epsilon^p x,\epsilon^p y,t;\epsilon^2 t)+\epsilon^2\mathbf{A}_{j2}+\cdots)e^{i\phi_j(\mathbf{x},t;\epsilon^{p+2}t)/\epsilon}, \tag{46}$$

where the amplitude envelopes $\mathbf{A}_{jk}$ vanish within the radius R and where the value of p relates the viscous length scale to R. Our analysis regards only the time evolution of the amplitudes $\mathbf{A}_{j1}(0,0,t,\epsilon^2 t)$ at the stagnation point. The mean-flow correction $\mathbf{U}_{2+p}$ scales with the terms $\Sigma_j\overline{\mathbf{A}}_{j1}\cdot\nabla\mathbf{A}_{j1}$ +c.c. at order ϵ^{2+p}. In the model flow, R is infinite and one is formally allowed to consider solutions that do not decay at infinity, i.e., $p=+\infty$. Nevertheless, when $p=0$ for the global flow, there is a mean-flow correction $\mathbf{U}_2$ at order ϵ^2 which influences the amplitudes at the order ϵ^3 equations. For example, such mean flow would modify the constants in our Eqs. (28)–(31) and perhaps inhibit the exponential growth of CCWs. Also, our cubic equations would become somewhat similar to the ones described by Waleffe[19] and Sipp.[20] In contrast, when $p\geq 1$ for the global flow, the mean-flow correction $\mathbf{U}_{2+p}$ is of a higher asymptotic order and it would influence the development of the cubic-order *unsaturated* states at longer timescales.

The numerical solution of Eq. (34) is a difficult numerical problem, as discussed in Appendix B. For example, with initial condition as a CCW plus a random disturbance, the numerical calculations show increasingly steep peaks. The near-zero amplitudes emerge from a background that starts at the initial disturbance and becomes progressively smaller. The integration in the presence of the steep peaks can be overcome with an implicit method, but even this goes only until the near-zero amplitudes become as small as the machine precision. If this scale separation continues to widen, no finite-precision computer can follow such stiff orbit. As a matter of fact, we were able to resolve the numerical calculation of the orbit of Fig. 4 only up to $T=5$.

For the true nonlinear dynamics of Eq. (35) with a dis-

Downloaded 17 Nov 2009 to 200.136.239.153. Redistribution subject to AIP license or copyright; see http://pof.aip.org/pof/copyright.jsp

turbed CCW initial condition, the long-term dynamics is very nontrivial. The steepening could saturate after a time scale or the scale separation could proceed indefinitely, either way representing a very peculiar dynamical behavior. The situation is similar to the dynamics generated by unstable critical points connected by heteroclinic orbits where the critical points lie on the coordinate axis. The peculiar behavior arises because here each axis is an orbit that tends to infinity. Another interesting dynamic emerges if there is a random noise added to the equations. In this case the near-zero amplitudes emerge at approximately the same scale, and there is stabilization-by-noise.

ACKNOWLEDGMENTS

This work was supported by the CNPq.

APPENDIX A: PROOF THAT SOME NONLINEAR TERMS VANISH

In the following, we prove that $\mathcal{N}^{+}_{11'}=\mathcal{N}^{+}_{22'}=0$ in Eq. (16). This is a consequence of the divergence-free condition and the subharmonic property of $\mathbf{p}_1(t)$. The relations between the components of $\mathbf{k}_j=(k_{xj},k_{yj},k_{zj})$ and $\mathbf{k}_{j'}=(k_{xj'},k_{yj'},k_{zj'})$ are $k_{xj'}=-k_{xj}$, $k_{yj'}=-k_{yj}$, and $k_{zj'}=k_{zj}$. It is known[7] that the periodic solution of Eq. (6) $\mathbf{p}_1=(p_{x1},p_{y1},p_{z2})$ has a subharmonic property among its components: $p_{x1}(t-P/2)=p_{x1}(t)$, $p_{y1}(t-P/2)=p_{y1}(t)$, and $p_{z1}(t-P/2)=-p_{z1}(t)$. Then, the components of $\mathbf{w}^0_j=(w^0_{xj},w^0_{yj},w^0_{zj})$ and $\mathbf{w}^0_{j'}=(w^0_{xj'},w^0_{yj'},w^0_{zj'})$ are related by $w^0_{xj'}=w^0_{xj}$, $w^0_{yj'}=w^0_{yj}$, and $w^0_{zj'}=-w^0_{zj}$. From Eq. (8) it follows that $v^0_{xj'}=v^0_{xj}$, $v^0_{yj'}=v^0_{yj}$, and $v^0_{zj'}=-v^0_{zj}$. Thus, $\mathbf{k}_{j'}\cdot\mathbf{w}^0_j=-\mathbf{k}_j\cdot\mathbf{w}^0_j$, and $\mathbf{k}_{j'}\cdot\mathbf{v}^0_j=-\mathbf{k}_j\cdot\mathbf{v}^0_{j'}$. From Eq. (16), it follows that the x and y-components of $\mathcal{N}^{+}_{jj'}$ are zero while the z-component is $2((\mathbf{k}_j\cdot\mathbf{w}^0_{j'})v^0_{zj}-(\mathbf{k}_j\cdot\mathbf{v}^0_{j'})w^0_{zj})$. Moreover, it is a standard property that the nonlinear term $\mathbf{u}\cdot\nabla\omega-\omega\cdot\nabla\mathbf{u}$ is divergence-free. This can be used to show that $\mathbf{k}_9\cdot\mathcal{N}^{+}_{jj'}=0$. Since $\mathbf{k}_9=(0,0,2\cos\theta_c)$, the z-component of $\mathcal{N}^{+}_{jj'}$ is also zero, and this completes the proof.

APPENDIX B: LONG-TERM NUMERICAL INTEGRATION

The numerical integration of Eq. (34) becomes prohibitive if we want to study its long-term evolution in order to assert the saturation of the growth-and-decay cycles. The example of Fig. 4 shows cycles among the wave amplitudes but there is a scale separation between the largest component of $\mathbf{y}(T)$ and the other near-zero components. It is noticeable that the exponential growth of a near-zero amplitude is what stops the growth of the dominant amplitude. The total growth for the near-zero amplitude depends on its initial value, which is seen to become progressively smaller. A formidable numerical problem occurs because this scale separation tends to increase very quickly in time, as shown in Fig. 6. When the scale separation becomes overwhelming for the machine precision, not even the correct qualitative behavior is attained. For example, the qualitative behavior of the stiff ODE integrator used in Fig. 6 eventually shows the exponential growth of a single-component CCW as if the near-zero amplitudes were in fact zero. On the other hand, an explicit Runge–Kutta method shows that the cycle amplitudes saturate at a certain height, when in fact, the near-zero amplitudes are being regarded as noise (numerical noise) at a fixed small level. In this case, the growth-and-decay cycles do persist, but their saturation is a stabilization by noise instead of the correct dynamical behavior. Fortunately, the numerical calculations can be carried with enough precision until $T=5$ so that the instability of a CCW and the subexponential growth of the cycles can be established. Moreover, for a real fluid, the time-asymptotic saturation level of the cycles is irrelevant, since either the weakly nonlinear approximation breaks down or the near-zero amplitudes reach the noise level present in the flow, whichever happens first.

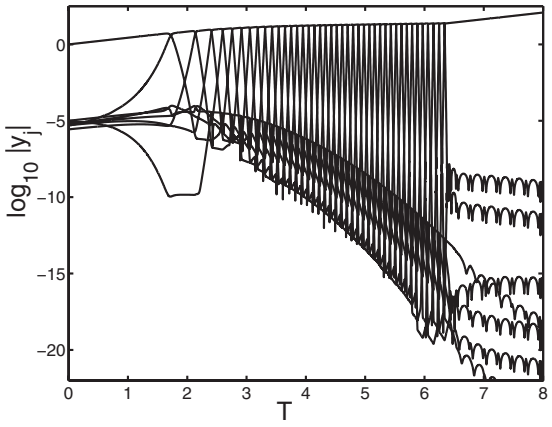


FIG. 6. Instability of a CCW for $T\in[0,8]$ where each line represents one component $\log_{10}|y_j(T)|$ for $j=0,\ldots,7$; the values of n, β, and ξ, and initial condition are the same as in Fig. 4. The near-zero components start at order 10^{-5} and become smaller until machine precision is reached at $T\approx 5.5$. Then, at $T\approx 6.4$, the near-zero components are neglected by the numerical integrator (as if they were zero) and a CCW becomes the numerically stable solution.

[1] R. R. Kerswell, "Elliptical instability," Annu. Rev. Fluid Mech. **34**, 83 (2002).
[2] R. T. Pierrehumbert, "Universal short-wave instability of two-dimensional eddies in an inviscid fluid," Phys. Rev. Lett. **57**, 2157 (1986).
[3] B. J. Bayly, "Three-dimensional instability of elliptical flow," Phys. Rev. Lett. **57**, 2160 (1986).
[4] D. D. Craik and W. O. Criminale, "Evolution of wavelike disturbance in shear flows: a class of exact solutions of the Navier–Stokes equation," Proc. R. Soc. London, Ser. A **406**, 13 (1986).
[5] M. J. Landman and P. G. Saffman, "The three-dimensional instability of strained vortices in a viscous fluid," Phys. Fluids **30**, 2339 (1987).
[6] A. Lifschitz and E. Hameiri, "Local stability conditions in fluid dynamics," Phys. Fluids A **3**, 2644 (1991).
[7] F. A. Waleffe, "On the three-dimensional instability of strained vortices," Phys. Fluids A **2**, 76 (1990).
[8] F. Gallaire, D. Gérard-Varet, and F. Rousset, "Three-dimensional instability of planar flows," Arch. Ration. Mech. Anal. **186**, 423 (2007).
[9] D. M. Mason and R. R. Kerswell, "Nonlinear evolution of the elliptical

Downloaded 17 Nov 2009 to 200.136.239.153. Redistribution subject to AIP license or copyright; see http://pof.aip.org/pof/copyright.jsp

instability: an example of inertial wave breakdown," J. Fluid Mech. **396**, 73 (1999).
[10]J.-P. Racz and J. F. Scott, "Parametric instability in a rotating cylinder of gas subject to sinusoidal axial compression. Part 2. Weakly nonlinear theory," J. Fluid Mech. **595**, 291 (2008).
[11]A. Lifschitz and B. Fabijonas, "A new class of instabilities of rotating fluids," Phys. Fluids **8**, 2239 (1996).
[12]C. S. Hellberg and S. A. Orszag, "Chaotic behavior of interacting elliptical instability modes," Phys. Fluids **31**, 6 (1988).
[13]D. Sipp and L. Jacquin, "Elliptic instability in two-dimensional flattened Taylor-Green vortices," Phys. Fluids **10**, 839 (1998).
[14]D. Sipp, E. Lauga, and L. Jacquin, "Vortices in rotating systems: Centrifugal, elliptic and hyperbolic instabilities," Phys. Fluids **11**, 3716 (1999).
[15]F. Gallaire, M. Marquillie, and U. Ehrenstein, "Three-dimensional transverse instabilities in detached boundary layers," J. Fluid Mech. **571**, 221 (2007).
[16]J. S. Leontini, M. C. Thompson, and K. Hourigan, "Three-dimensional transition in the wake of a transversely oscillating cylinder," J. Fluid Mech. **577**, 79 (2007).
[17]E. Knobloch, A. Mahlov, and J. E. Marsden, "Normal forms for three-dimensional parametric instabilities in ideal hydrodynamics," Physica D **73**, 49 (1994).
[18]E. Beltrami, *Mathematics for Dynamic Modeling* (Academic, New York, 1987).
[19]F. A. Waleffe, "The 3D instability of a strained vortex and its relation to turbulence," Ph.D. thesis, MIT, 1989.
[20]D. Sipp, "Weakly-nonlinear saturation of short-wave instability in a strained Lamb–Oseen vortex," Phys. Fluids **12**, 1715 (2000).

Downloaded 17 Nov 2009 to 200.136.239.153. Redistribution subject to AIP license or copyright; see http://pof.aip.org/pof/copyright.jsp